ACTA NEUROBIOLOGIAE EXPERIMENTALIS

Research paper Acta Neurobiol Exp 2012, 72: 253–263

Photoacoustic tomography can detect cerebral hemodynamic alterations in a neonatal rodent model of hypoxia-ischemia

Craig B. Sussman[1*], Candace Rossignol[1], Qizhi Zhang[3], Huabei Jiang[3], Tong Zheng[2], Dennis Steindler[2], Linda Young[4], and Michael D. Weiss[1]

[1]Department of Pediatrics, *Email: craig.sussman@jax.ufl.edu, Departments of [2]Neurosurgery, [3]Biomedical Engineering, [4]Statistics, University of Florida, Gainesville and Jacksonville, Florida, USA

Hypoxic-Ischemic Encephalopathy (HIE) is one of the most recognized causes of neurological deficits in children. Cerebral blood flow (CBF) reductions, as seen with HIE, resulting in neuronal injury have not been evaluated in real-time. Photoacoustic Tomography (PAT) is a form of optical imaging which can detect cerebral hemodynamic alterations in a non-invasive, non-ionizing fashion via changes in hemoglobin optical absorption. Further, this technology has the potential to capture cerebral blood volume (CBV) fluctuations and perhaps CBF changes in real-time. We hypothesized that PAT can detect a reduction in cerebral hemoglobin optical absorption, and therefore CBF, in a neonatal model of hypoxia-ischemia. To investigate, P7 rats underwent right carotid artery ligation and exposure to 8% oxygen for 60 minutes while imaged with PAT every 20 minutes. Cerebral hemodynamic alterations, as measured by mean optical absorption (MOA), were calculated as a change from baseline. Global and regional MOA was analyzed using a linear mixed model. Global MOA was reduced within the right hemisphere as compared to the left during hypoxia. Regional differences in MOA were detected between the left and right sides for the middle and posterior cortical regions. Injury was confirmed using immunohistochemistry. We conclude that a reduction in global and regional MOA, and hence CBF, could be identified by PAT in a neonatal rat model of HIE. This is the first study described in the literature utilizing a neonatal rat model of HIE to demonstrate in vivo alterations in cerebral hemodynamics in a non-invasive and near real-time fashion.

Key words: Photoacoustic tomography, neonatal, cerebral blood flow, hypoxia-ischemia, neuroimaging, rodent model

Abbreviations

CBF – Cerebral Blood Flow;
CBV – Cerebral Blood Volume;
HIE – Hypoxic-ischemic Encephalopathy;
MOA – Mean Optical Absorption;
PAT – Photoacoustic Tomography

INTRODUCTION

Hypoxic-ischemic Encephalopathy (HIE) occurring during the perinatal period is one of the primary causes of severe, long-term neurological deficits in children. HIE is the brain manifestation of systemic asphyxia which occurs in approximately 2–4 per 1 000 live births (Vannucci 1997). A dominant feature in the pathophysiology of HIE is a reduction in cerebral blood flow (CBF) resulting in ischemia. Most often, the neurological insult is a consequence of myocardial dysfunction with resultant loss of cerebral autoregulation (Volpe 2008). This pathophysiologic sequence results in destructive neuronal injury with 20–50% of affected neonates expiring during the newborn period. Of the survivors, up to 25% exhibit severe, permanent neuropsychological handicaps in the form of cerebral palsy, with or without associated mental retardation, learning disabilities, or epilepsy (Vannucci 1997).

In a hypoxic-ischemic environment, the cerebrovascular autoregulation system of the neonate is less equipped to maintain homeostatic CBF. Thus, even mild alterations in CBF during or initially after a hypoxic-ischemic event may be associated with seri-

Correspondence should be addressed to C.B. Sussman
Email: craig.sussman@jax.ufl.edu

Received 27 April 2012, accepted 22 August 2012

ous neurologic complications (Pryds et al. 1990, Greisen 1992). It has been a long-standing challenge for neonatal clinicians to monitor cerebral perfusion and neurologic function at the bedside of a critically ill neonate. For the past decade, well accepted, conventional neuroimaging modalities, including magnetic resonance (MRI), computed tomography (CT), and cranial ultrasonography (CUS) have been the standard of care for evaluating infants with neurologic pathology. These studies are pertinent for a comprehensive evaluation of an infant who has succumbed to HIE, and the results of these images assist the clinician in defining the degree of brain injury, facilitate in management decisions and provide vital prognostic information (Rutherford et al. 1998, Volpe 2008). However, neonates with severe HIE have multiorgan-system involvement and are often too unstable to be transported to MRI and CT scans. In addition, these conventional neuroimaging studies provide only static clinical correlations and lack the ability to track the evolution of injury over time. Further, MRI occupies a considerable amount of time with difficult access to the infant and CT delivers a substantial amount of ionizing radiation that may be detrimental to the developing brain (Hall et al. 2004). CUS is a non-invasive, portable modality commonly employed to neonates with useful but limited ability to evaluate global cerebral hemodynamics. CUS does not reliably illustrate myelination, diffuse white matter injury and metabolic disease or metabolic disturbances, including hypoglycemia. Moreover, abnormalities at the brain's convexity including hemorrhages and cortical abnormalities, are not easily depicted on CUS (van Wezel-Meijler et al. 2010). A safe technique to detect brain injury, evaluate cerebral hemodynamics, and monitor clinical alterations in real-time fashion at the bedside of a critically ill neonate would provide valuable diagnostic and prognostic information when caring for infants with neurologic pathology.

Photoacoustic Tomography (PAT) is a promising technology which combines the merits of high ultrasonic resolution with strong optical contrast to produce a three-dimensional image. In PAT, biological tissue is illuminated *via* a short-pulsed laser beam to produce thermal and acoustic impulse responses. Locally absorbed light is converted into heat, which is further converted to a pressure rise *via* thermoelastic expansion of the tissue (Wang 2008), termed the photoacoustic effect. The photoacoustic wave is detected by an ultrasonic transducer which produces electric signals. These signals are then amplified, digitized and transferred to a computer, where an image is formed based on the differences in tissue optical absorption. At a 532 nm wavelength laser pulse, hemoglobin has the highest optical absorption of all cerebral tissues. Thus, PAT has the ability to utilize hemoglobin as an endogenous contrast agent, enabling extremely sensitive imaging of the cerebral vasculature (Wang et al. 2003). PAT has found applications in imaging breast cancer (Ku et al. 2005), melanoma (Wang 2008), osteoarthritis (Ishihara et al. 2006), assessing cerebral blood oxygen saturations (Stein et al. 2009), as well as evaluating neuro-vasculature with and without functional hemodynamic variations (Wang et al. 2003). PAT is noninvasive, non-ionizing, inexpensive and portable, making it an ideal neuroimaging modality for critically ill neonates in the intensive care unit. Further, neonates may prove to be ideal candidates for PAT due to their relatively thin skull and open anterior fontanelle. These unique anatomical properties create minimal optical and ultrasonic attenuation when compared to more robust adult skulls (Wang et al. 2008).

In this pilot study, we hypothesized that PAT can visualize global and regional cerebral hemodynamic alterations in a neonatal rat model of hypoxia-ischemia in near real-time. Variations in the optical absorption of hemoglobin is utilized to evaluate cerebral blood volume (CBV) and as a surrogate marker of CBF. Further, the ability of PAT to evaluate cerebral reperfusion was explored. Physiological parameters including peripheral oxygen saturations and heart rate values were evaluated during hypoxia and correlated to cerebral hemodynamic fluctuations. Lastly, we discuss how the use of PAT in combination with the rodent hypoxia-ischemia model may serve as a novel approach to further explore both cerebral hemodynamics as well as future therapeutic interventions for neonatal neurologic injury.

METHODS

All animal procedures were reviewed and approved by the Institutional Animal Care and Use Committee (IACUC) at the University of Florida under protocol number 200902511.

Rat model of hypoxia-ischemia

The Rice-Vannucci method to produce hypoxic-ischemic brain injury in the postnatal day 7 rat pup is based on the Levine preparation in the adult rat (Levine 1960) and consists of unilateral common carotid artery ligation followed by systemic hypoxia produced by the inhalation of 8% oxygen (Rice et al. 1981). In this model, blood flow to the ipsilateral cortex is not influenced by unilateral arterial occlusion alone. However, when unilateral carotid ligation is combined with hypoxic gas exposure, the hypoxic-ischemic injury is associated with a reduction in CBF throughout the ipsilateral cortex (Vannucci et al. 1988). Briefly, postnatal day 7 Sprague-Dawley rat pups were anesthetized with 4% isoflurane in an induction chamber and maintained with 2% isoflurane during the carotid artery ligation procedure. The pups were placed on a clay mold with soft restraints and were continuously in contact with a heating gel pad (Braintree Scientific, Inc. Braintree, MA) to maintain thermoneutrality. Sterile technique was observed throughout. A 0.5 cm skin incision was made in the right lateral neck adjacent to the trachea. The carotid artery was isolated and ligated *via* a low temperature electrocautery pen (Medtronics, Jacksonville, FL). The skin incision was closed with 3M™ Vetbond™ Tissue Adhesive (n-butyl cyanoacrylate). The pups were allowed to fully recover with their mother post-operatively. They remained in a thermo-neutral environment and nursed without difficulties. Once full recovery was accomplished, approximately two hours post ligation, the pups were prepared for the hypoxic exposure and neuroimaging via the PAT system (see PAT and imaging schematic sections below).

Photoacoustic tomography system

A mechanical scanning photoacoustic system with single acoustic transducer was employed for collecting the light-induced acoustic signals. Figure 1 illustrates the schematic of the system. The light source was a pulsed Nd:YAG laser (Altos, Bozeman, MT) with 4 ns pulse duration and 10 Hz repetition rate. The output pulse energy could be up to 360 mJ at a wavelength of 532 nm. The diameter of the laser beam was expanded to 30 mm by a lens and the light power was adjusted to 15 mJ cm^{-2} at the surface of the rat's head, which was lower than the maximum permissible exposure for skin to a 532 nm laser beam (20 mJ cm^{-2}). An immersion acoustic transducer with 1 MHz nominal frequency (Valpey Fisher, Hopkinton, MA) was driven by a motorized rotator to receive light-induced acoustic signals over

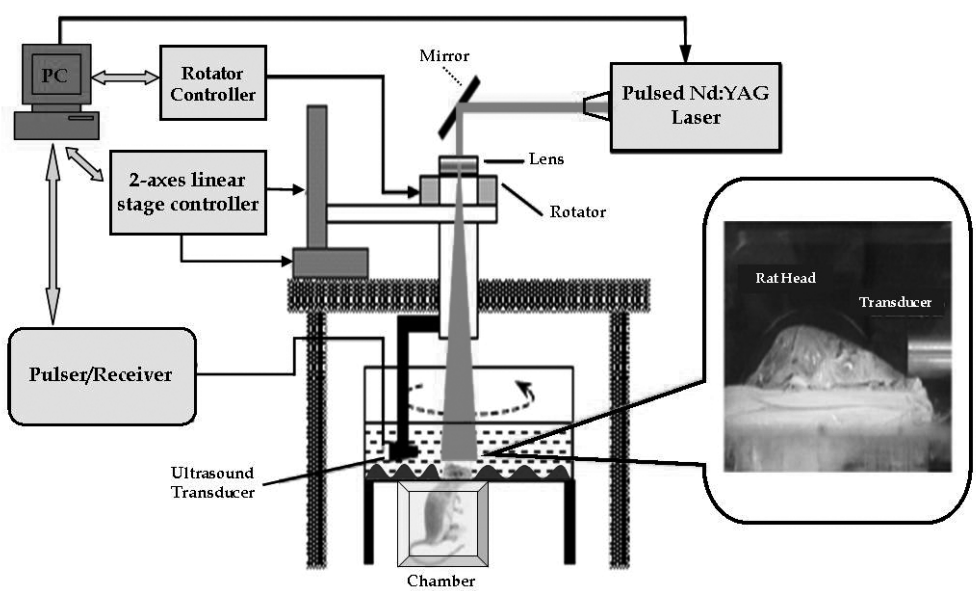

Fig. 1. Photoacoustic Tomography Schematic. The Nd:YAG laser pulses the mirror and is deflected through the lens onto the subject's skull. Light-induced optical absorption signals are collected *via* the ultrasound transducer, which is in communication with the pulser/receiver. The signals are interpreted by the computer generated algorithm to create a final PAT image. The inset is a close-up image of the head/water/transducer interface. (PAT) photoacoustic tomography.

360º at an interval of 6º in the horizontal plane and thus a total of 60 measurements were performed for one planar scanning. Approximately 4.5 minutes were required to complete each cycle. Scanning along the *z*-axis was accomplished by mounting the rotator and the transducer on a small platform driven by a linear stage. The acoustic transducer was immersed into the water tank, for signal amplification, while the rat's head was placed into the imaging field through an opening covered with a piece of polyethylene membrane at the bottom of the tank (Fig. 1 insert). The complex wavefield signal was amplified by a pulser/receiver (GE Panametrics, Waltham, MA) which worked in receiver mode only, and was then acquired by a high-speed PCI data acquisition board. A LabView program (National Instruments Corporation, Austin, TX) controlled the entire system. The spatial resolution of this scanning system in the *x*–*y* plane was 1 mm and the signal-to-noise ratio was improved by averaging signals from ten samplings at each detector position.

Reconstruction algorithm

The reconstruction approach in PAT in this study is an iterative Newton method with combined Marquardt and Tikhonov regularizations that can provide stable inverse solutions. The approach uses the hybrid regularizations-based Newton method to update an initial (guessed) optical property distribution iteratively in order to minimize an objective function composed of a weighted sum of the squared difference between computed and measured data. A detailed description of the algorithm has been previously published (Yuan et al. 2005). Briefly, time harmonic light-induced acoustic wave propagation in tissue can be described by the following Helmholtzlike equation:

$$\nabla^2 p(r,\omega) + k_0^2 p(r,\omega) = ik_0 \frac{c_0 \beta \Phi(r)}{C_p} \tag{1}$$

where p is the pressure wave; $k_0=\omega/c_0$ is the wavenumber described by the angular frequency ω and the speed of the acoustic wave in the medium, c_0; β is the thermal expansion coefficient; C_p is the specific heat; Φ is the product of the optical absorption coefficient and the excitation light distribution. To solve equation (1) with the finite-element method, p and Φ are defined as the sum of coefficients multiplied by a set of basic functions and we obtain the finite-element discretization of equation (1) and the associated boundary conditions:

$$\mathbf{Ap} = \mathbf{b\Phi} \tag{2}$$

$$(\Im^T \Im + \mathrm{I})\Delta \div = \Im^T (\mathbf{p}^o - \mathbf{p}^c) \tag{3}$$

where the elements of the matrix A and b are expressed as $a_{mn} = \int_V (\nabla \varnothing_m \cdot \nabla \varnothing_n - k^2 \varnothing_m \varnothing_n) dV + \int_\Gamma (-\varnothing_m \nabla \varnothing_n \cdot \mathbf{n}) d\Gamma$ and $b_{mn} = \int_V (-ik\beta c \varnothing_m \varnothing_n / C_p) dV$, respectively. p^o and p^c in equation (3) are the vectors representing observed

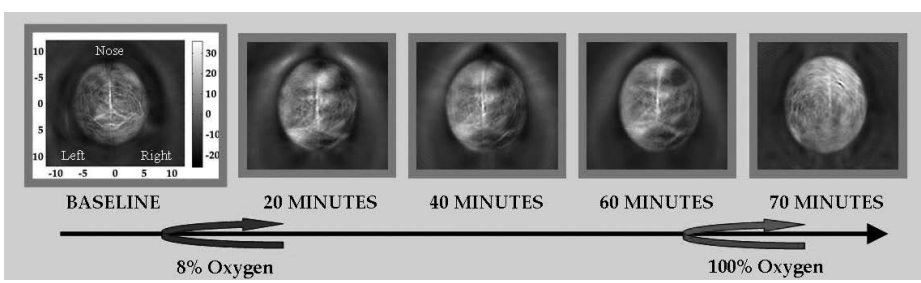

Fig. 2. Photoacoustic images during hypoxia and reperfusion. Axial view of reconstructed photoacoustic images demonstrating the distribution of optical absorption in the pup's cortex at baseline, during hypoxia (20, 40, and 60 min) and reperfusion (70 min). Hemoglobin has the highest absorption coefficient among all cerebral tissue at a wavelength of 532 nm. The gray scale (right of baseline image) represents the optical absorption of tissue (arbitrary units). The more white the pixel, the higher the absorption, and therefore more hemoglobin. After 20 minutes of hypoxia, the optical absorption in the right hemisphere decreases significantly as compared to the left hemisphere indicating a reduction in cerebral blood flow. The 70 minute image represents the ability of PAT to evaluate reperfusion; as there is a global increase in optical absorption after 10 minutes of hyperoxia (F_iO_2 100%). (PAT) photoacoustic tomography; (F_iO_2) fraction of inspired oxygen.

and computed complex acoustic field data at the boundary locations, respectively. $\Im$ is the Jacobian matrix formed by $\partial p/\partial \Phi$ at the boundary measurement sites, $\Delta\chi$is the update vector for the optical properties, λ is a scalar and I is the identity matrix. Based on iterative solution of Equations 2 and 3, the optical absorption distribution is updated in order to minimize the weighted sum of the squared difference between computed and measured data so that PAT images are reconstructed. Note that the recovered optical absorption has arbitrary units. The average of the optical absorption measurements for each time point is expressed as mean optical absorption (MOA).

Hypoxia-ischemia imaging schematic

Once the pups fully recovered from surgery they were placed in a chamber designed for PAT. The chamber, with a dimension of 11.4 cm × 7.6 cm × 12.7 cm, was constructed from translucent plastic with a soft foam interior where the pups were gently restrained. Intake and outtake gas hoses were attached to opposite poles of the chamber. The intake gas hose enabled humidified hypoxic gas (8% oxygen) to be infused into the chamber. This hose also allowed for an inhalation anesthetic to be infused at low doses (1–2% isoflurane) in order to minimize distress and limit the pup's activity throughout imaging. The outtake hose served to both eliminate pressure build up within the chamber and as an isoflurane scavenger. Chamber temperature was monitored with a portable digital thermometer (ACU-RITE®, Schaumburg, IL). Chamber thermo-neutrality was achieved by heating the tank water with a Theo 100 watt aquarium heater (Hydor USA, Sacramento, CA) and by the use of a heating gel pad (Braintree Scientific, Inc. Braintree, MA) placed under the chamber. Once anesthetized, PAT images were obtained at baseline prior to the induction of hypoxia by the schematic and algorithm described above. This enabled each pup to serve as their own control and as an experimental subject. PAT images were then recorded during hypoxia at intervals of 20, 40, and 60 minutes. Hemoglobin has the highest absorption co-efficient of all cerebral tissue at 532 nm. Therefore, higher concentrations of hemoglobin in a given brain region results in greater MOA values. The MOA values for each hemisphere were calculated by PAT measurements at baseline, 20, 40 and 60 minutes (Figs 2 and 4). Regional cerebral hemodynamics were interpreted from MOA maps by placing six individual voxels over the anterior, middle and posterior right and left cortical regions (R1, R2, R3, L1, L2, L3 in Fig. 3). MOA for each region was analyzed at the same time points described above. After the 60-minute image was obtained, the pups were exposed to 100% oxygen and final PAT measurements were recorded at 70 minutes to evaluate

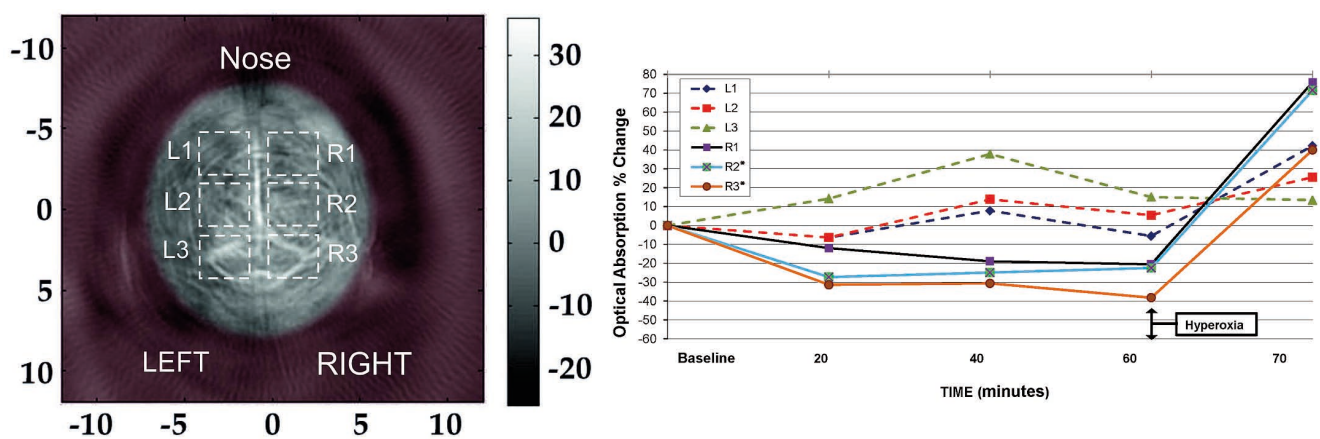

Fig. 3. Regional mean optical absorption over time. MOA in six cortical regions are plotted over time. Regions are labeled as L (left) 1–3 and R (right) 1–3. The image in the left panel is the superficial cortex at time zero or baseline prior to hypoxia. Regional changes in MOA during hypoxia and reperfusion are plotted on the right panel. Regional differences in MOA were detected between the left and right sides for regions 2 and 3 during hypoxia. Region R 3 had the most significant reduction in MOA during hypoxia. All regions return to or above their baseline values following hyperoxia (F_iO_2 100%). *Indicates regions with statistical significance ($P \leq 0.05$). (MOA) mean optical absorption; (F_iO_2) fraction of inspired oxygen.

cerebral reperfusion. The degree of cerebral hemodynamic fluctuation, measured numerically as MOA of brain tissue, was calculated and recorded based on the above reconstruction algorithm. In addition, peripheral oxygen saturations and heart rate values were monitored and recorded throughout the imaging process by MouseOx® Pulse Oximeter (STARR Life Sciences™ Corp, Oakmont, PA). Post-imaging, the pups fully recovered on a heating gel pad and were then returned to their mother to nurse. The subjects were monitored closely during the imaging process and until full recovery was accomplished.

Immunihistochemistry

Tissue Processing

Following survival times of 14 days (P21), animals were deeply anesthetized with isoflurane and perfused transcardially with 4% paraformaldehyde in 0.1 M phosphate buffered saline (PBS; ph=7.4). Brains were removed, postfixed overnight in perfusate, transferred to 30% sucrose for another 24 hours before sectioning in the coronal plane at a thickness of 40 μm with a freezing microtome.

Immunolabeling

For detection and localization of injury, tissue sections were processed for immunofluorescence with rabbit polyclonal antibody against GFAP (1:1000, Dako) and mouse monoclonal antibody against Beta III tubulin, (1:1000; Clontech). Sections were incubated overnight at 4°C in primary antibodies diluted in PBS containing 10% fetal bovine serum and 0.1% Triton X-100. Sections were then rinsed and incubated at room temperature for two hours with fluorescence-labeled secondary antibodies (Oregon Green anti-rabbit IgG and CY3 anti-mouse IgG) before being mounted, coverslipped with mounting media with 4',6-diamidino-2-phenylindole (DAPI), and evaluated with epifluorescence (Fig. 5).

Statistical analysis

Global and regional differences in cerebral hemodynamics, measured as a change from baseline of MOA, between the left and right cortex over time were analyzed using a linear mixed model. The study was conducted as a randomized complete block design with repeated measures over time (20, 40, and 60 minutes).

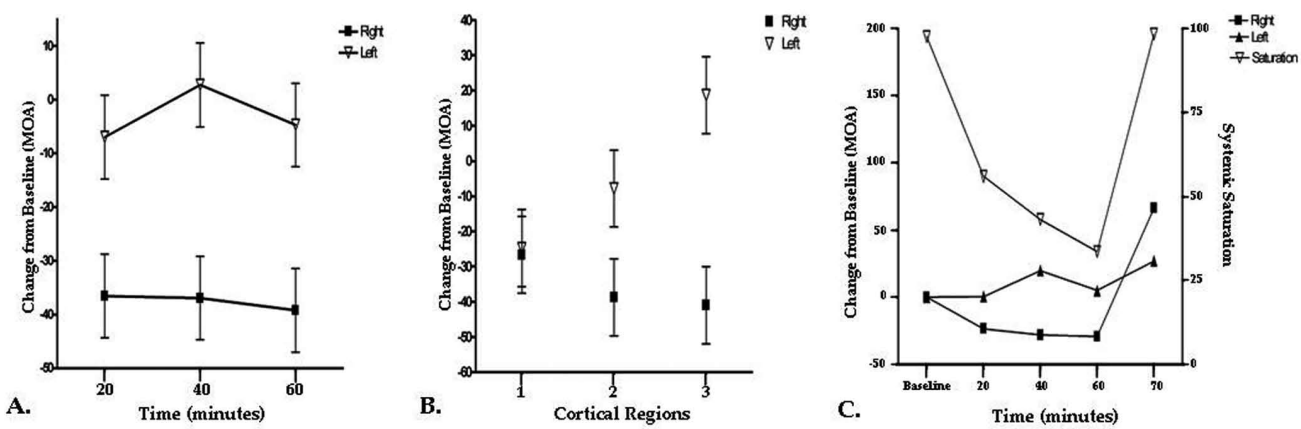

Fig. 4. Changes in MOA from baseline during hypoxia [Global (A), Regional (B) and in relation to systemic saturations(C)]. (A) Right vs. Left hemisphere MOA change from baseline during hypoxia. MOA in the right hemisphere decreases significantly as compared to the left hemisphere during hypoxia. (B) Regional differences in MOA as a change from baseline value. The combined regional average MOA at the 20, 40, and 60 minute time points were compared to the average baseline MOA. Differences in MOA were detected between the left and right sides for region 2 and for region 3. (C) Relationship between systemic SaO_2 and MOA within the right and left hemisphere hypoxia and reperfusion. No statistical correlation was detected between SaO_2 and MOA within the right or left hemisphere. Graphically, as SaO_2 decrease, MOA within the right hemisphere is reduced during hypoxia and recovers during reperfusion. Note, MOA within the left hemisphere remains relatively stable throughout the experiment. (MOA) mean optical absorption; (SaO_2) systemic oxygen saturations.

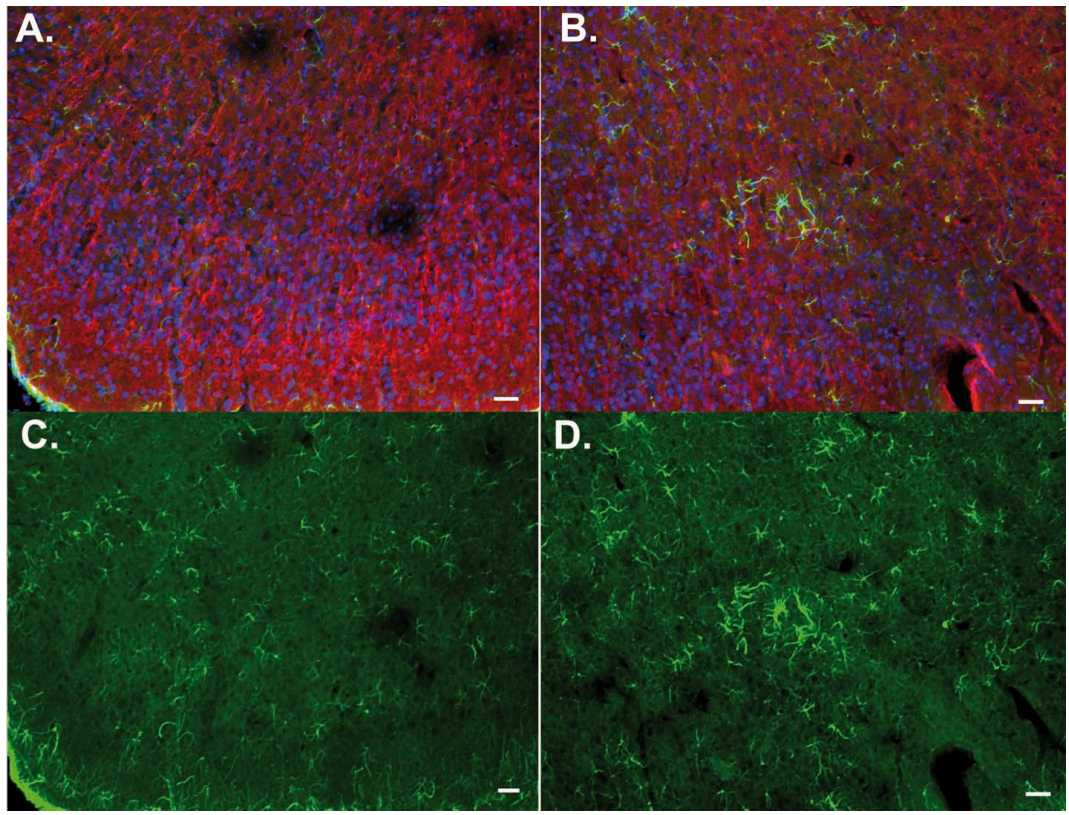

Fig. 5. Cortical immunohistochemistry 14 days post systemic hypoxia-ischemia. Sections are stained with GFAP (green), βIII Tubulin (red) and counter-stained with DAPI (blue). Panels (A) and (C) were obtained from the left (non-ligated) cortex while Panels (B) and (D) were obtained from the right (ligated/injured) cortex. GFAP in green represents reactive gliosis with increased astrocyte number and reactive processes in the right cortex as compared to the left. A decrease in βIII Tubulin (red) was observed in the right cortex illustrating a reduction in neuronal density. Scale bar is 200 μm.

Because measurements from the same pup were anticipated to be more alike than measurements from different pups, each pup was taken to be block, which was the random effect. The two factors, side (L and R) and region (1, 2, 3), were crossed. A Toeplitz covariance structure accounted for the correlation among observations collected over time from the same pup. Four animals were utilized in the statistical analysis with a total of 72 observations for all regions and time points. A 5% significance level was used for all tests. Lastly, potential correlations between cerebral MOA, heart rate and systemic oxygen saturations during hypoxia were investigated using Pearson's correlation coefficients.

RESULTS

Analysis of global cerebral hemodynamics demonstrated the MOA to be significantly less within the right hemisphere as compared to the left hemisphere during hypoxia at all time points ($F_{1,25.9}$= 12.55, P=0.0015) (Fig. 4A). Measurement of MOA also differed between right and left cortical regions during the hypoxic exposure. As illustrated in Figure 4B, differences in MOA were detected between the left and right sides for region 2 ($t_{25.9}$=2.05, P=0.050) and for region 3 ($t_{25.9}$=3.96, P=0.0005). No significant disparity in MOA was noted between the left and right sides for region 1 ($t_{25.9}$=0.13, P=0.901).

No significant correlations were observed between MOA in the right (ligated) hemisphere and heart rate values (r=0.511(4), P=0.489) or systemic oxygen saturations (r=−0.459(4), P=0.540) during hypoxia. Further, no significant correlation was observed for the MOA in the left hemisphere and heart rate (r=0.304(4), P=0.695) or systemic saturations (r=0.762(4), P=0.237) during the hypoxic exposure. However, a trend was observed as systemic saturations decreased. During systemic hypoxia, the MOA within the right (ligated) hemisphere was reduced and recovered after 10 min-

utes of hyperoxia. MOA within the left hemisphere remained relatively stable throughout the experiment. These findings are graphical displayed in Figure 4C. Note, Figure 4C is void of error bars in order to present the trend since findings were not statistically significant.

Immunohistochemistry of the cortex at 14 days post surgery revealed mild injury on the side of the carotid ligation; consistent with the short hypoxic exposure in this injury model (Fig. 5). Diffuse reactive gliosis and a sporadic decrease in Beta III tubulin staining was observed on the ligated (right) cortex compared to the non-ligated (left) cortex (Fig. 5B, D). These findings were consistent with the duration of hypoxic exposure which produces a mild injury (Towfighi et al. 1991).

DISCUSSION

Development of an ideal neonatal neuroimaging modality is an ongoing challenge within the world of neonatal intensive care medicine. Innovations including low radiation, rapid CT and diffusion-weighted MRI have changed the approach to which infants with neurologic dysfunction are evaluated and managed. Despite these advances, we continue to lack the ability to non-invasively detect and follow structural and functional variations in real-time at the bedside of a critically ill neonate. As presented in this paper, PAT has the potential to overcome some of the above mentioned obstacles. We have demonstrated that in near real-time PAT can visualize alterations in cerebral hemodynamics during hypoxia-ischemia and reperfusion. Utilizing PAT, we have further illustrated that the hemodynamic reductions were not in fact symmetric throughout the right hemisphere, but had the most dramatic reduction in the right posterior, superficial brain region. The more severe ischemia visualized in the right posterior superficial cortex is consistent with regional CBF flow studies utilizing positron emission tomography in term neonates with HIE (Volpe et al. 1985, Shah et al. 2001). As speculated by others, this is likely a contributing factor to the common occurrence of parasagittal brain injury observed in neonatal HIE, especially posterior.

The correlation of visual and statistical ipsilateral cerebral hemodynamic alterations in near real-time by PAT further supports the well established rodent model of hypoxia-ischemia as an ideal surrogate for studying neonatal brain injury. The Rice-Vannucci model of unilateral carotid artery ligation of the P7 rat pup to induce brain injury has been utilized in laboratories worldwide since the early 1980's. In this model, histological brain injury is general confined to the cerebral hemisphere ipsilateral to the arterial occlusion, and consists of selective neuronal death or infarction depending on the duration of systemic hypoxia (Vannucci and Vannucci 2005). Using this model, researchers have explored a variety of physiologic manipulations including hypothermia, hypo/hyperglycemia, hypo/hypercapnia and hypoxic preconditioning to alter the degree of cortical injury (Vannucci and Vannucci 2005).

In the rodent model of hypoxia-ischemia, brain injury is an almost universal finding in the immature rats surviving 1–3 hours of systemic hypoxia. After that time, appreciable mortality occurs (Vannucci et al. 1999). Our lab has demonstrated, in past experiments, the ability to replicate and explore this model successfully. In our current study, we aimed to evaluate cerebral hemodynamics, and thus a more limited exposure to hypoxia was undertaken. Using this approach, we were capable of evaluating hemodynamics while maintaining survival in our subjects.

Measurements of cerebral blood flow in the model have been described by using carbon-14 autoradiography with iodo-[14C]-antipyrine. This technique has demonstrated that blood flow to the ipsilateral cortex was not influenced by unilateral arterial occlusion alone. However, when unilateral carotid ligation is combined with hypoxic gas exposure, the hypoxic-ischemic injury is associated with a reduction in CBF throughout the ispilateral cortex (Vannucci et al. 1988). Additional studies have assessed CBF distribution and resultant grade of hypoxia-ischemia by means of a non-radioactive, colored microsphere technique. With this technique, retention of microspheres in capillaries of the brain tissue enabled the investigators to simultaneously study the morphological and blood flow distribution in the newborn rat model (Xia et al. 2002). Although these techniques are valuable and suitable for determining CBF distribution on a histological basis, they do not allow for *in-vivo* analysis. Prior to our described study, cerebral hemodynamics in the HIE rodent model has not been evaluated in near real-time. Our study was able to demonstrate *in vivo,* ipsilateral changes in cerebral hemodynamics in a non-invasive and near real-time fashion. Because PAT

detects alterations in hemoglobin, one may assume that a reduction in the PAT signal correlates with a reduction in CBV. Although it cannot be verified using the current PAT technique, histological evidence of ipsilateral injury in the regions of decreased MOA, and a reduction in MOA from the baseline values supports that not only CBV was diminished, but also CBF. While PAT indirectly measures CBF alterations by its ability to capture variations in hemoglobin, its application in evaluating cerebral hemodynamic changes may prove useful clinically and experimentally. Thus, the use of PAT in combination with the rodent hypoxia-ischemia model may serve as a novel approach to further explore both cerebral hemodynamics as well as future therapeutic interventions for neonatal neurologic injury.

The ability to maintain cerebral autoregulation, a constant CBF over a range of perfusion pressures, is critical to protect the developing brain from ischemic injury. Autoregulation in an adult human is over a range of mean arterial blood pressures between approximately 60 and 150 mmHg (Lassen 1959). The range of mean arterial blood pressures in which a neonate operates is unknown and controversial. However, it is thought that neonatal cerebral autoregulation functions over a much lower and narrower range than adults and is strongly influenced by gestational age (Nuntnarumit et al. 1999, Seri and Evans 2001). Since there is no current modality to continuously evaluate cerebral hemodynamics at the bedside, the point at which cerebrovascular autoregulation is assumed to be disrupted is the most widely accepted physiological definition of clinical systemic hypotension (Seri 2001).

Near-infrared spectroscopy (NIRS) has demonstrated potential as a bedside cerebral monitoring device within the neonatal intensive care unit. Supportive evidence using NIRS demonstrated that hypotension and blood pressure fluctuations increase the incidence of intraventricular hemorrhage and periventricular leukomalacia in preterm infants and that cerebral oxygenation is dependent on systemic blood pressure (Tsuji et al. 2000). Although commercially available NIRS can provide valuable information regarding regional cerebral saturations, it is only capable of evaluating mixed cerebral saturations across a broad area, displaying a numerical value, and not visual insight into global cortical hemodynamic status. Experimentally, using NIRS-based technology, optical tomography enables three-dimensional visualization of the optical properties of the brain.

This technology has revealed an incidence of intraventricular hemorrhage, changes in CBV, and measurements of oxygenation induced by small alterations in ventilator settings (Hebden et al. 2002). However, optical tomography faces many limitations including poor spatial resolution beyond the soft depth limit from strong diffusion due to tissue scattering (Wang 2008), slow acquisition times and reconstruction speed, and high cost (Minagawa-Kawai et al. 2008). On the other hand, photoacoustic technology has been shown to provide similar oxygen saturation data in rodents with the addition of superior cerebral vasculature imaging (Stein et al. 2009). Utilizing photoacoustic imaging, further insight into many neonatal dilemmas, including exploring the ideal mean arterial blood pressure required to maintain adequate cerebral perfusion, may be addressed.

A number of factors contribute to cerebrovascular autoregulatation including hydrogen and potassium ions, adenosine, carbon dioxide, oxygen tension as well as other variables (Volpe 2008). In our current study, we attempted to correlate systemic oxygen saturations and cerebral hemodynamic alterations measured as MOA by the PAT system. Prior experiments have demonstrated that decreases in oxygen tension result in an increase in CBF. The mechanism responsible for this increase is thought to be related to an increase in local factors including hydrogen ions, potassium and adenosine (Jones and Traystman 1984). After prolonged hypoxia, CBF eventually falls as a result of myocardial failure with associated systemic hypotension (Volpe 2008). Our study observed an initial increase, followed by a preservation of left (nonligated) hemispheric MOA values during systemic hypoxemia, likely due to the above mentioned vasodilatory factors. Although vasodilatation likely also occurred in the right cortex, the right carotid artery ligation limits right hemispheric CBF.

Vannucci and Vannucci's original neonatal rodent hypoxia-ischemia model illustrated a reduction in carbon dioxide into the mid-twenties (mmHg) while maintaining a relatively normal pH for up to 180 minutes of hypoxia (Vannucci and Vannucci 2005). Although preferred, due to the technical limitations of subject size and the inability to access the rodent in the PAT chamber, our group was unable to feasibly obtain carbon dioxide measurements. We therefore depended

on the results in the original experiments, and assumed carbon dioxide levels decreased during the 60 minutes. It is for these same limitations that mean arterial blood pressure measurements were not record in this study. Of interest, MOA measured by PAT in the right hemisphere was reduced as systemic oxygen saturations declined. The inability to statistically correlate the degree of systemic hypoxemia with MOA reduction in the right hemisphere may be due to the small sample size analyzed. A future study, with a more robust sample size may validate the degree of systemic hypoxia as a surrogate marker of cerebral ischemic severity when employed in this model. In addition, future alterations in our PAT set-up may allow for blood sampling and pressure measurements.

Technical limitations of this model included rat pup cortical size in relation to photoacoustic signal optimization, movement artifact during PAT, and the requirement of multiple images to create a MOA for each time point over 4.5 minutes. For example, to create each final image per time point, 60 individual signals were acquired and combined at 6 degree intervals. Approximately 4.5 minutes were required to complete each cycle. Therefore, cerebral hemodynamic observations could only be measured as a mean, and images were therefore generated as near real-time. In order to rectify this issue, a multi-array scanner will need to be employed to enable an image to be captured with its corresponding optical absorption at a single point in time. Another limitation is the potential for cortical hyperthermia as a result of photoacoustic technology. As the laser is pulsed, a slight increase in internal tissue temperature occurs. Previous studies have estimated a <20 mK temperature increase occurring in the local skin during PAT (Wang et al. 2003), however, the cortical temperature change is unknown. Although this elevation in temperature is theoretically insignificant, future studies will need to strictly evaluate internal brain temperature fluctuations, especially if this technology is to be implemented in neonates undergoing hypothermia as a neuroprotective therapy.

To obtain photoacoustic signal optimization, the water tank was required to surround the pup's skull due to its minute size (Fig. 2). When PAT is employed in a larger animal model or a neonate, water will not be required, but only ultrasound gel applied to the neonate's head to obtain signal optimization. Therefore, in theory, a neonate will be able to lay supine and uninterrupted during the imaging session. Lastly, we employed a wavelength of 532 nm which is optimal for hemoglobin absorption and penetration of a P7 rat skull. Studies have indicated that longer wavelengths, in the range of 680 nm to 950 nm, are required to effectively penetrate cadaveric, human neonatal skulls (Wang et al. 2008). Future experiments, utilizing a larger animal model, will aim to evaluate the ideal wavelength to both maximize hemoglobin optical absorption and achieve adequate depth of penetration.

CONCLUSION

Reduction in global and regional cortical MOA, and hence cerebral hemodynamics, could be identified *in-vivo,* for the first time, by PAT in a neonatal rat model of HIE. As the technology of PAT is refined, a multi-array scanner is generated, and larger neonatal animal hypoxia-ischemia models are utilized we will move closer to creating the ideal neuroimaging modality for human neonates. Future and on-going PAT studies will work towards the common goal of safely incorporating PAT as a non-invasive, real-time method to evaluate cerebral hemodynamic status, assess cortical injury and assist in developing neuroprotective strategies within the walls of the neonatal intensive care unit.

ACKNOWLEDGEMENT

This work was supported by National Institutes of Health (NIH) NS052583-01A2 (MDW) and NIH/NINDS grant NS055165 and the Maren, Thompson and McKinney Regeneration Funds to DS.

REFERENCES

Greisen G (1992) Effect of cerebral blood flow and cerebrovascular autoregulation on the distribution, type and extent of cerebral injury. Brain Pathol 2: 223–228.

Hall P, Adami HO, Trichopoulos D, Pedersen NL, Lagiou P, Ekbom A, Ingvar M, Lundell M, Granath F (2004) Effect of low doses of ionising radiation in infancy on cognitive function in adulthood: Swedish population based cohort study. BMJ 328: 19.

Hebden JC, Gibson A, Yusof RM, Everdell N, Hillman EM, Delpy DT, Arridge SR, Austin T, Meek JH, Wyatt JS (2002) Three-dimensional optical tomography of the premature infant brain. Phys Med Biol 47: 4155–4166.

Ishihara M, Sato M, Kaneshiro N, Mitani G, Sato S, Mochida J, Kikuchi M (2006) Development of a diagnostic system for osteoarthritis using a photoacoustic measurement method. Lasers Surg Med 38: 249–255.

Jones MD Jr., Traystman RJ (1984) Cerebral oxygenation of the fetus, newborn, and adult. Semin Perinatol 8: 205–216.

Ku G, Fornage BD, Jin X, Xu M, Hunt KK, Wang LV (2005) Thermoacoustic and photoacoustic tomography of thick biological tissues toward breast imaging. Technol Cancer Res Treat 4: 559–566.

Lassen NA (1959) Cerebral blood flow and oxygen consumption in man. Physiol Rev 39: 183–238.

Levine S (1960) Anoxic-ischemic encephalopathy in rats. Am J Pathol 36: 1–17.

Minagawa-Kawai Y, Mori K, Hebden JC, Dupoux E (2008) Optical imaging of infants' neurocognitive development: recent advances and perspectives. Dev Neurobiol 68: 712–728.

Nuntnarumit P, Yang W, Bada-Ellzey HS (1999) Blood pressure measurements in the newborn. Clin Perinatol 26: 981–996.

Pryds O, Greisen G, Lou H, Friis-Hansen B (1990) Vasoparalysis associated with brain damage in asphyxiated term infants. J Pediatr 117: 119–125.

Rice JE, 3rd, Vannucci RC, Brierley JB (1981) The influence of immaturity on hypoxic-ischemic brain damage in the rat. Ann Neurol 9: 131–141.

Rutherford MA, Pennock JM, Counsell SJ, Mercuri E, Cowan FM, Dubowitz LM, Edwards AD (1998) Abnormal magnetic resonance signal in the internal capsule predicts poor neurodevelopmental outcome in infants with hypoxic-ischemic encephalopathy. Pediatrics 102: 323–328.

Seri I (2001) Circulatory support of the sick preterm infant. Semin Neonatol 6: 85–95.

Seri I, Evans J (2001) Controversies in the diagnosis and management of hypotension in the newborn infant. Curr Opin Pediatr 13: 116–123.

Shah S, Fernandez AR, Chirla D (2001) Role of brain SPECT in neonates with hypoxic ischemic encephalopathy and its correlation with neurodevelopmental outcome. Indian Pediatr 38: 705–713.

Stein EW, Maslov K, Wang LV (2009) Noninvasive, in vivo imaging of blood-oxygenation dynamics within the mouse brain using photoacoustic microscopy. J Biomed Opt 14: 020502.

Towfighi J, Yager JY, Housman C, Vannucci RC (1991) Neuropathology of remote hypoxic-ischemic damage in the immature rat. Acta Neuropathol 81: 578–587.

Tsuji M, Saul JP, du Plessis A, Eichenwald E, Sobh J, Crocker R, Volpe JJ (2000) Cerebral intravascular oxygenation correlates with mean arterial pressure in critically ill premature infants. Pediatrics 106: 625–632.

van Wezel-Meijler G, Steggerda SJ, Leijser LM (2010) Cranial ultrasonography in neonates: role and limitations. Semin Perinatol 34: 28–38.

Vannucci RC, Lyons DT, Vasta F (1988) Regional cerebral blood flow during hypoxia-ischemia in immature rats. Stroke 19: 245–250.

Vannucci RC (1997) Hypoxia-ischemia: Clinical aspects. In: Neonatal-Perinatal Medicine IV (Fanaroff AA, Martin RJ, Eds). Mosby-Yearbook, Inc., Philadelphia, PA, p. 877–891.

Vannucci RC, Connor JR, Mauger DT, Palmer C, Smith MB, Towfighi J, Vannucci SJ (1999) Rat model of perinatal hypoxic-ischemic brain damage. J Neurosci Res 55: 158–163.

Vannucci RC, Vannucci SJ (2005) Perinatal hypoxic-ischemic brain damage: evolution of an animal model. Dev Neurosci 27: 81–86.

Volpe JJ, Herscovitch P, Perlman JM, Kreusser KL, Raichle ME (1985) Positron emission tomography in the asphyxiated term newborn: parasagittal impairment of cerebral blood flow. Ann Neurol 17: 287–296.

Volpe J (2008) Neurology of the Newborn. Saunders, Philadelphia, PA.

Wang LV (2008) Prospects of photoacoustic tomography. Med Phys 35: 5758–5767.

Wang X, Chamberland DL, Xi G (2008) Noninvasive reflection mode photoacoustic imaging through infant skull toward imaging of neonatal brains. J Neurosci Methods 168: 412–421.

Wang X, Pang Y, Ku G, Xie X, Stoica G, Wang LV (2003) Noninvasive laser-induced photoacoustic tomography for structural and functional in vivo imaging of the brain. Nat Biotechnol 21: 803–806.

Xia YX, Sameshima H, Ikeda T, Higo T, Ikenoue T (2002) Cerebral blood flow distribution and hypoxic-ischemic brain damage in newborn rats. J Obstet Gynaecol Res 28: 320–326.

Yuan Z, Wu C, Zhao H, Jiang H (2005) Imaging of small nanoparticle-containing objects by finite-element-based photoacoustic tomography. Opt Lett 30: 3054–3056.